

1 **The choice of baseline period influences the**
2 **assessments of the outcomes of Stratospheric Aerosol**
3 **Injection**

4 **D. Vioni^{1,2}, E. M. Bednarz^{3,4,5}, D. G. MacMartin⁵, B. Kravitz^{6,7} and P. B.**
5 **Goddard⁶**

6 ¹Department of Earth and Atmospheric Sciences, Cornell University, Ithaca, NY, USA

7 ²Atmospheric Chemistry Observations & Modeling, National Center for Atmospheric Research, Boulder,
8 CO, USA

9 ³Cooperative Institute for Research in Environmental Sciences (CIRES), University of Colorado Boulder,
10 Boulder, CO, USA

11 ⁴NOAA Chemical Sciences Laboratory (NOAA CSL), Boulder, CO, USA

12 ⁵Sibley School of Mechanical and Aerospace Engineering, Cornell University, Ithaca, NY, USA

13 ⁶Department of Earth and Atmospheric Sciences, Indiana University, Bloomington, IN, USA

14 ⁷Atmospheric Sciences and Global Change Division, Pacific Northwest National Laboratory, Richland,
15 WA, USA

16 **Key Points:**

- 17 • We analyze results from a set of simulations considering various amounts of cool-
18 ing using stratospheric aerosols.
19 • Many of the climatic responses at the surface can be considered linearly related
20 to the amount of cooling.
21 • The choice of the specific baseline period influences these conclusions.

Corresponding author: Daniele Vioni, dv224@cornell.edu

Abstract

The specifics of the simulated injection choices in the case of Stratospheric Aerosol Injections (SAI) are part of the crucial context necessary for meaningfully discussing the impacts that a deployment of SAI would have on the planet. One of the main choices is the desired amount of cooling that the injections are aiming to achieve. Previous SAI simulations have usually either simulated a fixed amount of injection, resulting in a fixed amount of warming being offset, or have specified one target temperature, so that the amount of cooling is only dependent on the underlying trajectory of greenhouse gases.

Here, we use three sets of SAI simulations achieving different amounts of global mean surface cooling while following a middle-of-the-road greenhouse gas emission trajectory: one SAI scenario maintains temperatures at 1.5°C above preindustrial levels (PI), and two other scenarios which achieve additional cooling to 1.0°C and 0.5°C above PI.

We demonstrate that various surface impacts scale proportionally with respect to the amount of cooling, such as global mean precipitation changes, changes to the Atlantic Meridional Overturning Circulation (AMOC) and to the Walker Cell. We also highlight the importance of the choice of the baseline period when comparing the SAI responses to one another and to the greenhouse gas emission pathway.

This analysis leads to policy-relevant discussions around the concept of a reference period altogether, and to what constitutes a relevant, or significant, change produced by SAI.

Plain Language Summary

By adding CO₂ to the atmosphere, the planet warms. As the primary energy input to the system is the Sun, you can try to balance this warming by slightly reducing the incoming sunlight, for example by adding tiny reflecting particles to the atmosphere (aerosols). This cooling will not perfectly cancel the warming from CO₂ due to different physical mechanisms. Understanding how the resulting climate from both effects changes requires a comparison with a "base" state: but there isn't one single choice, something which is made even more clear once one considers multiple amounts of cooling one could do. There isn't only one option as one could decide to just prevent future warming (or some of it), or also try to cancel warming that already happened. Here we explore how the projected outcomes can depend on the base state one selects and which change are linear with the amount of cooling achieved.

1 Introduction

The adverse global impacts produced by human-induced surface warming are well-documented in over 30 years of previous scientific literature and international proceedings. In 1990, the first Intergovernmental Panel on Climate Change (IPCC) Assessment Report already highlighted many of the future challenges and laid the ground for the creation of the United Nations Framework Convention on Climate Change (UNFCCC). The second Assessment Report, in 1995, was essential in informing policy makers on their way to approve the Kyoto Protocols in 1997, where the first legally binding commitment to reduce emissions (by 5% compared to 1990 levels) was ratified. By the time of the Fourth and Fifth assessment reports, observations of rising greenhouse gas (GHG) emissions and concentrations and increasing surface temperatures led the scientific community and the parties of the UNFCCC to determine new emission commitments. These commitments were not just based on emission targets, but also on global mean temperature "thresholds" that the world should commit to not trespassing during this century in order to avoid the worst effects of climate change (Gao et al., 2017). The Paris Agreement clearly stated that the parties were bound (Rajamani & Werksman, 2018) to limit global warm-

ing to well below 2, and pursue efforts to limit temperature increase to 1.5 °C, compared to pre-industrial levels. The need for such thresholds was highlighted in the IPCC Special Report on Global Warming of 1.5°C (Masson-Delmotte et al., 2018), where the risks of staying below 1.5°C as compared to 2°C was discussed in depth.

More recently, multiple studies have shown how countries' commitments and actions are faring against these temperature targets determined in the Paris Agreement, with the general agreement being that almost none of the signatories are actually close to achieving the emission cuts necessary in the short term to remain below 1.5°C (e.g., Kriegler et al. (2018); Brecha et al. (2022)). The current IPCC emission scenarios that maintain temperatures below this threshold (with or without a temporary overshoot) make use of large assumptions of the scalability and deployability of carbon dioxide removal (CDR) technologies in the future (Haszeldine et al., 2018), which some have criticized as unrealistic (Holz et al., 2018; Boettcher et al., 2021; Warszawski et al., 2021). This non-exhaustive and brief description of the last decades of climate change serves here to highlight a conundrum: the risks of surface temperatures going above 1.5°C above preindustrial get clearer with every passing year, and that temperature threshold risks being reached in the next two decades, yet, actual emission cut pledges by all nations that would serve to curtail that warming are not matching what is in international agreement, and the need for a rapid ramping up of CDR necessary to avoid an overshoot (Kriegler et al., 2018) is not matched by current developments in that area.

A potential additional element of a policy response in the short term, allowing for temperatures (and risks) to be managed while emissions are reduced was already discussed by (Crutzen, 2006) with the proposal to reduce a portion of the incoming sunlight by means of injecting sulfate aerosol precursors into the lower stratosphere (Stratospheric Aerosol Injections, SAI hereafter), in order to produce an optically active cloud of aerosol particles with a long lifetime. Crutzen already highlighted risks as well: not only those in the physical realm (changes in stratospheric composition, differences in the forcing of GHG and of the produced aerosols resulting in a climate different from that produced by a reduction of GHG concentrations) but also those in the human and policy realm, namely that the idea itself of SAI could interfere with emission abatements because of the perception that an “easier” option is available. Research in the last two decades has tried to better understand both of those kinds of risks. In the physical sphere, this has been done mainly by simulating the potential effects of simplified SAI deployment scenarios in global climate models, either by injecting some quantity of SO₂ or of other aerosols in the tropical lower stratosphere (Robock et al., 2008; Kravitz et al., 2015), or by simply reducing the solar constant at the top of the model as a proxy (Niemeier et al., 2013; P. Irvine et al., 2019; Visoni, MacMartin, Kravitz, Boucher, et al., 2021; Visoni, MacMartin, & Kravitz, 2021).

In order to understand the impacts of global warming – which ultimately depend on how much greenhouse gas is emitted – the IPCC usually evaluates multiple future scenarios. As the effects of SAI similarly depend on how it is done (e.g., Kravitz et al. (2019)), one cannot make conclusions about the impacts of SAI by only analyzing one scenario. In terms of the magnitude of cooling to achieve, different areas of the world might desire different amounts, and that simply slowing down the warming (MacMartin et al., 2018; P. Irvine et al., 2019), or keeping it at the Paris Agreement threshold of 1.5°C above preindustrial might not be enough for them to stave off the worst or most long term impacts from climate change such as sea level rise (P. J. Irvine et al., 2012). Trade offs between larger coolings and larger impacts from stronger interventions need to be better determined: in (MacMartin et al., 2022) we explained the rationale behind our new sets of simulations which will be used in this work, in which we compare a scenario where, under SSP2-4.5 emissions, SAI is used to keep temperatures at 1.5°C above preindustrial with two other scenarios that further cool by 0.5°C and 1.0°C below that level.

Here we further explore our set of scenarios, leveraging the combination of different comparison periods and of scenarios with different cooling amounts to discuss both the linearity of the surface climate response and to highlight how important the choice

of a reference period is when discussing the potential outcomes of SAI. In the following section we will briefly describe the climate model used for this study and then explain more in depth the functioning of the feedback algorithm that determines how to inject SO_2 to achieve the temperature targets in the three SAI scenarios (Section 2). We will then discuss the outcomes in terms of sulfate burden (Section 3.1), surface temperature (Section 3.2) with a focus on the tropical Eastern Pacific response (Section 3.2.1), Atlantic Meridional Overturning Circulation (Section 3.3) and global and regional precipitation (Section 3.4; these all provide examples where the choice of reference period influences interpretations.

2 Methods

2.1 Climate model

In this study we use the Community Earth System Model Version 2 (CESM, Danabasoglu et al. (2020)) in its Whole Atmosphere Community Climate Model Version 6 (WACCM6) configuration with simplified tropospheric chemistry (Davis et al., 2022), hereafter CESM2-WACCM6. This model version has a horizontal resolution of 1.25° longitude by 0.9° latitude with 70 vertical levels that extend up to about 140km. The version we use has comprehensive stratospheric and upper-atmospheric chemistry, as well as an interactive aerosol microphysics scheme termed the Modal Aerosol Module (MAM4) (Liu et al., 2016), but has simplified tropospheric chemistry that only includes the most relevant processes and does not have detailed Secondary Organic Aerosol (SOA) chemistry; in (Davis et al., 2022), this has been shown to not produce relevant changes in stratospheric chemistry and surface climate.

2.2 Simulations design

We consider here three SAI scenarios spanning the period 2035 to 2070, each of which injects the appropriate (more details provided shortly) SO_2 magnitudes required to keep global mean surface temperatures at 1.5°C , 1.0°C or 0.5°C above the preindustrial levels (PI, with the 2020-2039 mean of the CESM model surface temperature data defined as corresponding to the 1.5°C above PI), respectively (henceforth referred to as SAI-1.5, SAI-1.0, SAI-0.5); motivation and description is given in MacMartin et al 2022. In all cases, GHG emissions follow the Shared Socioeconomic Pathway (SSP) 2-4.5 (Meinshausen et al., 2020).

The SO_2 is injected at every time step, every day of the year at 4 off-equatorial locations - 30°N , 15°N , 15°S and 30°S , and the yearly injection rates are determined independently at the beginning of each year using a feedback algorithm as in Kravitz et al. (2017). The algorithm computes the injection rates by comparing the annual mean near-surface air temperatures simulated over the previous year to determine how much those values differ from the desired target. This is done not just for global mean near-surface temperature (T0) but also the difference in temperatures between the two hemispheres, computed using the projection of the zonal mean surface temperature onto the first Legendre polynomial (eq. here), and the difference in temperatures between the poles and the equator, computed using the projection onto the second Legendre polynomial ($\ell_0 = 1$, $\ell_1 = \sin(\psi)$, and $\ell_2 = 3(\sin^2(\psi) - 1)/2$, where ψ is the latitude). The target values can be tied to periods in the baseline simulations when T0 had the same 20-year average value: so for SAI-1.5, the period over which T0 is 1.5°C above PI is 2020-2039 (by definition of our simulations). For SAI-1.0 and SAI-0.5, these periods are 2008-2027 and 1993-2012, respectively, which corresponds to T0 values that are 0.5°C and 1.0° lower than for the SAI-1.5. Determining this time-period of reference is necessary to calculate the target values for T1 and T2: for all scenarios, these two targets are the values averaged over the reference period.

174 The controller algorithm uses these targets to determine the needed yearly injection
 175 rates of SO_2 at the four latitudes, by estimating the needed projections of the zonal
 176 mean stratospheric aerosol optical depth (sAOD) onto the same Legendre polynomials
 177 to achieve them and then estimating the injections rates necessary to achieve those sAOD
 178 patterns. Information on how the injection of a certain amount of SO_2 translated to a
 179 certain shape of sAOD and to a certain temperature response are derived from single-
 180 point sensitivity simulations that have been described in Visoni et al. (2023), where all
 181 information is available to reproduce the calculations with similar sensitivity simulations
 182 in other climate models. The presence of the feedback algorithm is not trying to repre-
 183 sent how operationally SAI would work in the real world but should be viewed instead
 184 as a modeling tool to allow us to “learn” the set of injection rates needed to achieve a
 185 given set of targets.

186 In all cases, we analyze the responses over the last 20 years of the SAI simulations
 187 (i.e. 2050-2069), and compare them against each of the respective baseline periods with
 188 the same global mean surface temperature, as well as against the same quasi-present day
 189 period, here chosen as the mean over 2020-2039.

190 2.3 Simulated injection rates

191 In Figure 1 we show the connection between the imposed SO_2 injection rates and
 192 the resulting sAOD patterns and the magnitudes of the global mean cooling. In the top
 193 part, we show the total injection rates in the three sets of simulations. In the case of the
 194 SAI-1.5 simulation the target (1.5°C above PI) is reached just a few years before the start
 195 of SAI in 2035; therefore the injection rate can be allowed to slowly build up to offset
 196 the corresponding global warming (Fig. 1a). In contrast, for SAI-1.0 and SAI-0.5 a “ramp-
 197 up” time of 10 years has been built in in the controller to gradually achieve the desired
 198 temperature target (and so to avoid a steep temperature change over a few years). Af-
 199 ter that, changes in injection rates are similar to SAI-1.5, i.e. to just offset the warm-
 200 ing from GHGs in SSP2-4.5.

201 While global mean temperature changes can be tied to the overall injection rates,
 202 the management of the other two targets (T1 and T2) depend on the distribution of in-
 203 jection rates over the four locations. Figure 1b shows this distribution as a fraction of
 204 the overall injection rates (thereby accounting for the differences in total magnitudes).
 205 The distribution of the injection rate during the second part of the simulation (after the
 206 initial 10 years) depends on the ratio $dT1/dT0$ and $dT2/dT0$ (calculated as the value
 207 of T in the reference period minus that in the 2050-2069 period and shown in Table S1),
 208 which in turns affect the L1/L0 and L2/L0 ratio needed, which influences the amounts
 209 at the various injection locations (MacMartin et al., 2017). In all three cases over half
 210 of the injection is determined to be at 15°S and 15°N, and the remnant at 30°S, with
 211 no injection at 30°N. The distribution of injection rates at the onset of SAI is not nec-
 212 essarily consistent in the first 10 years, i.e before the controller converges, as the initial
 213 period is influenced by the convergence time of the algorithm and by the initial best guess
 214 (based on the sensitivity to the fixed injection rates shown in Visoni et al. (2023)). The
 215 hemispheric asymmetry in injection rates is discussed (for simulations in slightly differ-
 216 ent model configuration) in (Fasullo & Richter, 2023).

217 In panels 1c-e), we show the projections of the achieved sAOD patterns on the first
 218 three Legendre polynomials (termed L0, L1, L2), which relate to the overall magnitude
 219 of injection (panel 1a) for L0 and to the locations of the injections for L1 and L2, which
 220 indicate how much difference there is in sAOD between the hemispheres (L1) and be-
 221 tween tropical and high latitudes (L2) (Ban-Weiss & Caldeira, 2010). In Fig. S1, we also
 222 show the relationship between the actual sAOD and the internal control variables indi-
 223 cating the expected values by the controller based on the response in the fixed injection.
 224 If the relationship between injection rates and L0, L1, L2 remained linear, then the ex-
 225 pected L0, L1, L2 would match the actual. Fig. S1 shows that while the match is very
 226 good for SAI-1.5, for higher temperature targets the controller assumes that less SO_2 is

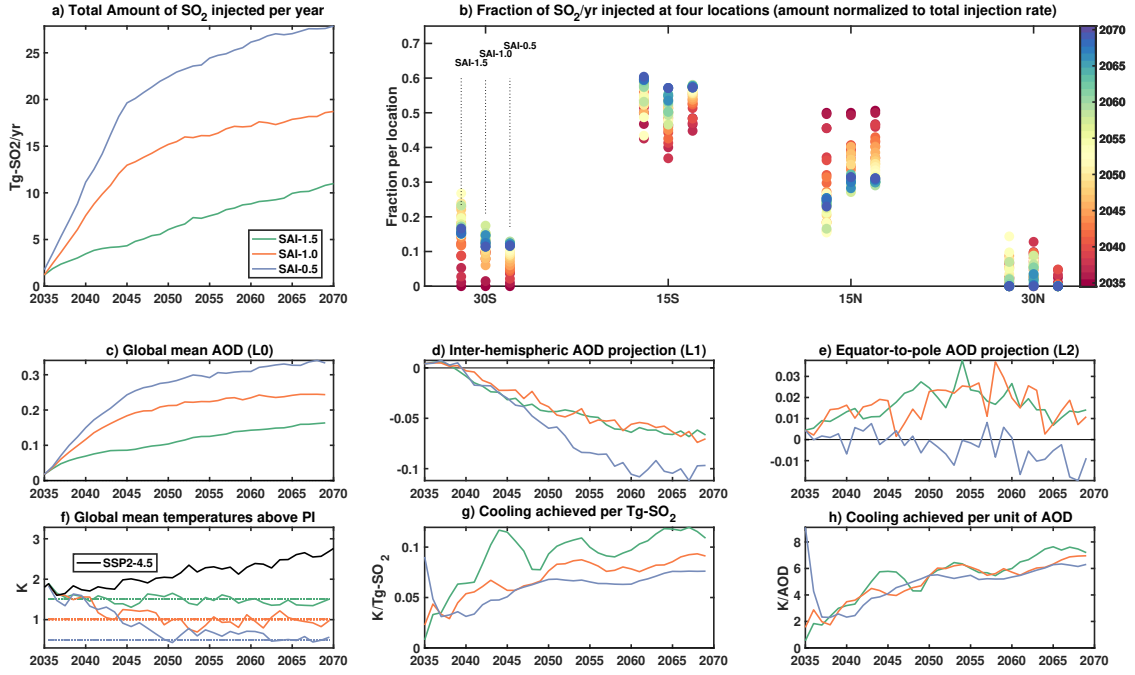


Figure 1. a) Total injection rates in the three sets of SAI simulations. b) Distribution of the injection rates at the four injection locations (30°S, 15°S, 15°N, 30°N), shown as the fraction of the total amount, color-coded depending on the year from red (2035) to blue (2070); SAI-1.5 is always the leftmost set, followed by SAI-1.0 and SAI-0.5. c-e) Values of L0 (global mean sAOD), L1 (inter-hemispheric sAOD projection) and L2 (equator-to-pole sAOD projection). f) Global cooling achieved in the SAI simulations compared to preindustrial (PI) temperatures. g) Efficacy of cooling per 1 Tg of SO₂ injected. h) Efficacy of cooling per sAOD produced. A 5-years running mean is applied to panels (g) and (h). For clarity, only the ensemble averages are shown in all panels.

needed to achieve a certain sAOD pattern. This points to nonlinearities in the injection rate to AOD conversion under high injection rates, which could arise from larger effective radii and shorter aerosol lifetime (particularly for L0) and from dynamical changes in the stratospheric transport (for L1 and L2) due to stronger lower stratospheric warming in the tropics (Visioni, MacMartin, Kravitz, Lee, et al., 2020). The differences in L1 for SAI-0.5 are driven by a value of $dT1/dT0$ (Table S1) that is 28% larger compared to that in SAI-1.5; similarly, the L2 differences are driven by a $dT2/dT0$ value that is 25% smaller in SAI-0.5 compared to SAI-1.5.

Figure 1f shows the simulated global mean temperatures above PI conditions and, thus, illustrates the overall cooling achieved in the three simulations compared to the warming in the SSP2-4.5 scenario (also shown in MacMartin et al. (2022)). Over the last 20 years of the three SAI simulations, the difference in global mean temperatures compared to the same period in SSP2-4.5 is 0.9 °C (SAI-1.5), 1.4 °C (SAI-1.0) and 1.8 °C (SAI-0.5). Finally, in panels g) and h) we show how this cooling relates to the injected amount of SO₂ and to the unit of global mean AOD. We find that the relationship between the total SO₂ injection and the resulting global mean cooling is sublinear (i.e. the strongest efficacy is found for SAI-1.5); similarly, a lower cooling per unit AOD is achieved, with a value of 6.5, 6.1 and 5.7 K/AOD for SAI-1.5, SAI-1.0 and SAI-0.5 respectively. Both sublinearities are due to microphysical nonlinearities (Niemeier & Timmreck, 2015; Visioni, MacMartin, Kravitz, Lee, et al., 2020) as larger aerosols have lower lifetime as they're heavier and they are also less efficient scatterer (Laakso et al., 2022). Hence, while 10 Tg-SO₂ are necessary in SAI-1.5 to cool by 1°C, the next 10 Tg-SO₂ only cool by 0.7°C in SAI-0.5, thereby requiring 26 Tg-SO₂ to cool to the desired target of 1.8 °C, instead of 18 Tg-SO₂ if the relationship had remained the same as in SAI-1.5.

3 Results

3.1 Sulfate burden

In Figure 2 we show the changes in the stratospheric sulfate burden produced by the injections described in Section 2.3. A comparison of panels a-c) highlights the large differences in the sulfate concentrations between the three SAI strategies, in line with the differences in cooling and injection rates reported in Fig. 1. SAI-1.5 increases the sulfate burden by up to 40 $\mu\text{g-S/kg-air}$ in the tropical lower stratosphere (as compared to 1 $\mu\text{g-S/kg-air}$ in the unperturbed stratosphere, while SAI-0.5 peaks at 108 $\mu\text{g-S/kg-air}$). Similarly, the overall increase in column burden as shown in panel 2d is 20.2 mg-S/m² for SAI-1.5 and 52.6 mg-S/m² for SAI-0.5. Despite large differences in total sulfate burden, all 3 SAI simulations show similar horizontal distributions with the largest sulfate burden (Fig. 2d) and sAOD (Fig. 2e) increases in the Southern Hemisphere, consistent with the similarities in the distributions of the injection rates in Fig. 1b. The significantly larger (by a factor of ~ 2) amount of aerosols in the Southern Hemisphere than the Northern Hemisphere is necessary in this model version in order to manage the inter-hemispheric temperature gradient (see Fasullo and Richter (2023) for details and for a discussion of differences with CESM1).

Fig. 2f and 2g, together with Fig. 1g and 1h further inform whether the achieved cooling is linear with respect to increasing injection rates. Fig. 2g indicates that in the three scenarios the injection rates and produced AOD are proportional, but the coefficient of the linear fit between the three is different because of dynamics in the first part (higher injections in the first years mean that AOD needs some years before it converges) and because of microphysical nonlinearities in the second. Therefore, if one only had the SAI-1.5 simulation, and assumed linearity and excluded the first 10 years as SO₂ to AOD converges, they would conclude that it would take 24 Tg-SO₂ to achieve a global AOD of 0.3, whereas in SAI-0.5 it takes 26, an 8% error. Similarly, Fig. 1h and Fig. 2g show that the same unit of AOD results in a slightly different amount of cooling: 6 K per unit of AOD globally, in SAI-1.5, and 7 in SAI-0.5), a 14% difference. Overall, both sub-linearities

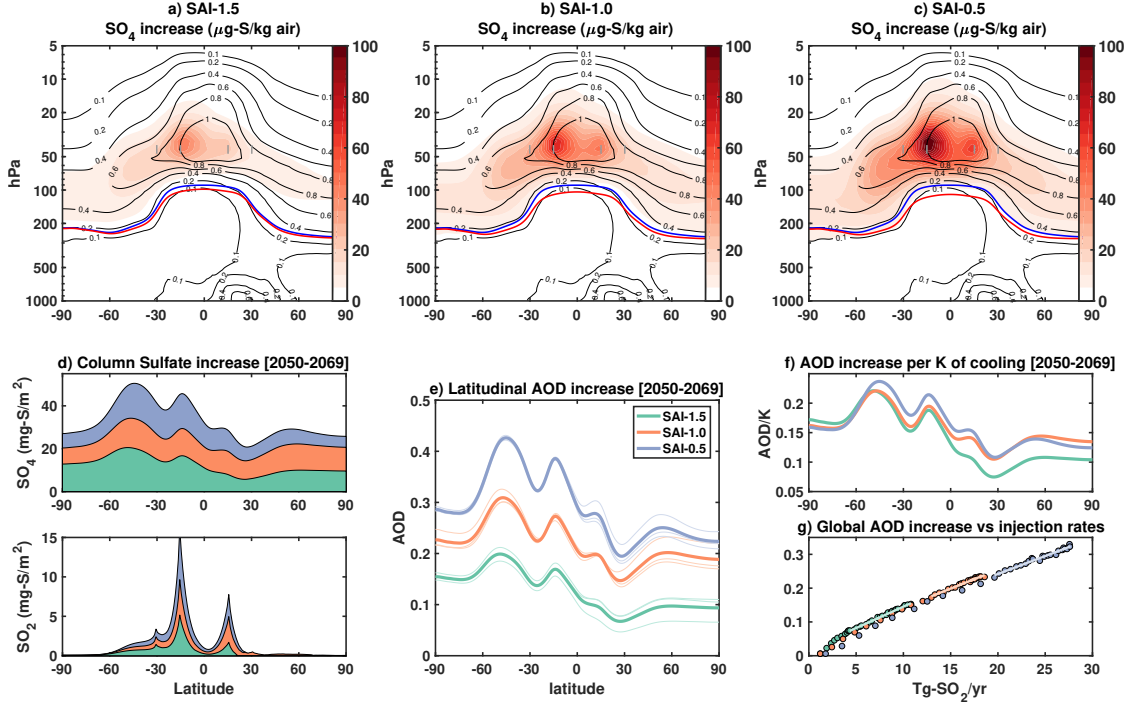


Figure 2. a-c) Shading: Zonal mean increase in sulfate mass concentrations (in $\mu\text{g-S/kg-air}$) for the 2050-2069 period in the three SAI experiments (SAI-1.5, SAI-1.0 and SAI-0.5 compared to the 2020-2039 period in the background SSP2 simulation (shown as thin contour lines). Blue line indicates the average annual tropopause height in the background SSP2 simulation for the 2020-2039 period, red lines indicate the same quantity for the three respective SAI simulations over 2050-2069. d) Zonal mean increase in the overall column burden in the three simulations for SO_4 (top) and SO_2 (bottom) for 2050-2069. e) Zonal mean stratospheric optical depth (sOD) increase for 2050-2069, lighter lines show single ensemble realizations. f) Zonal mean increase in stratospheric optical depth (sAOD) normalized by the resulting cooling over the same period. g) global mean AOD as a function of SO_2 injected in the same year.

279 compound in those found in Fig. 1g and discussed in Section 2.3, resulting in a 31% er-
 280 ror in estimating the required injection to achieve the cooling in SAI-0.5 based on the
 281 SAI-1.5 simulations.

282 3.2 Temperature response

283 An important question when discussing the possible surface response to SAI is “What
 284 should simulations of SAI be compared against?”. We offer as an example one previous
 285 comparison available in the literature: the GeoMIP G6sulfur simulation protocol (Kravitz
 286 et al., 2015). This simulation protocol used a scenario following the SSP5-8.5 emissions
 287 and prescribed an intervention where SAI was applied to bring temperatures down to
 288 those in a scenario following the SSP2-4.5 emissions. For a future period simulated with
 289 SAI, one could thus compare a certain quantity (mean temperature, mean precipitation,
 290 frequency or intensity of a type of extreme event) against both SSP5-8.5 and SSP2-4.5
 291 and observe which spatial differences are present in G6sulfur minus SSP2-4.5, and con-
 292 trast them with those between SSP5-8.5 and SSP2-4.5.

293 In our case, our set of simulations can help us expand this comparison by being more
 294 explicit on what our goals are. The central problem with GHG-induced global warm-

ing (as a measure of other changes) is that it shifts the climatic state outside of historical climate variability, it does so too fast for ecosystems and human adaptation capabilities, and it risks approaching irreversible changes in the system (i.e. tipping points, Lenton et al. (2008)). The comparison of a future (SSP2-4.5) and past period helps identify these changes, with different future GHG concentration levels dictating the amount of warming (Meinshausen et al. (2020), not shown here). SAI introduces a new dimension, as the stratospheric aerosol cooling, on top of increasing GHG concentrations, can reduce the increase of global mean temperatures, stop it, or even cool down to a previous level compared to present days. Evaluations of the SAI+GHG scenarios can thus compare them against:

1. Future periods without SAI, but with the same GHG concentrations (and higher global temperatures), which is relevant for comparative impact assessment.
2. Present day period, hence with lower GHG concentrations, which highlights differences with currently experienced climate by highlighting “deviations” from a (somewhat arbitrarily chosen) baseline state, though deviations from this state do not directly convey information about impacts.
3. Periods with same global mean temperature, but lower GHG concentrations (with the same caveats). Depending on the SAI scenarios, some of these periods might overlap or hold different meanings: in the G6sulfur example, (3) also indicates a future period, but with less warming because of the underlying SSP scenario, and “present day” is cooler than both.

In the cases under analyses here, SAI-1.5 cools by construction exactly at the “present day” level (2020-2039), while SAI-1.0 and SAI-0.5 cool further, allowing for a three point comparison between SSP2-4.5, SAI and baseline cases. Finally, instead of selecting just one “baseline” with a strict comparison of periods with the same global mean temperature, one can compare against a larger portion of the historical period, focusing on understanding when the compensation of GHG warming with SAI cooling results in a state that lies in a certain range of historical variability.

Examples of comparisons as outlined above are given in Figure 3 for the spatial distribution of temperature changes in the last 20 years of simulation. Top row panels show the regional effects of global temperature warming under SSP2-4.5 by comparing the future period with present or past periods with lower global mean temperature. Comparing SSP2-4.5 with ‘present day’ (2020-2039, BASE-1.5) already shows changes detectable everywhere on the globe, with a global average increase of 1.3 °C. By comparing the same time period in the SAI-1.5 simulation against this reference, we can observe how “effective” our simulated SAI strategy is in offsetting the GHG-induced warming. Using a double-sided t-test to determine statistical significance at a 95% level, temperature changes would be detectable only in 27% of the world compared to BASE-1.5. As the 1.5 °C threshold is, in many ways, arbitrary, one can also choose to compare against other periods, such as when temperatures were cooler, e.g. the 2008-2027 (BASE-1.0) and 1993-2012 (BASE-0.5). If SAI only cools globally by 0.8 °C (as in the SAI-1.5 simulation), then most areas will still be warmer than 0.5°C above PI. A similar statement can be made for the other simulations and other possible reference periods. In Fig. 3 we highlight this aspect by representing the overall space of possible comparisons using a matrix approach in which rows represent any future simulation (either SSP2-4.5, SAI-1.5, SAI-1.0 or SAI-0.5) and the columns represent a potential target to compare our future simulation against.

The diagonal panels in Fig. 3 show changes in SAI-1.5, SAI-1.0 and SAI-0.5 against their target periods, BASE-1.5, BASE-1.0 and BASE-0.5 (i.e. the periods in the past with the same 20-year-mean global mean temperature). This comparison highlights that more cooling results in more areas that show statistically significant temperature changes. Among these changes is a temperature increase over the Eastern Pacific, projecting onto the pattern associated with the positive phase of the El-Nino Southern Oscillation (ENSO), and a temperature decrease over the Northern Atlantic, indicating a weakening of the At-

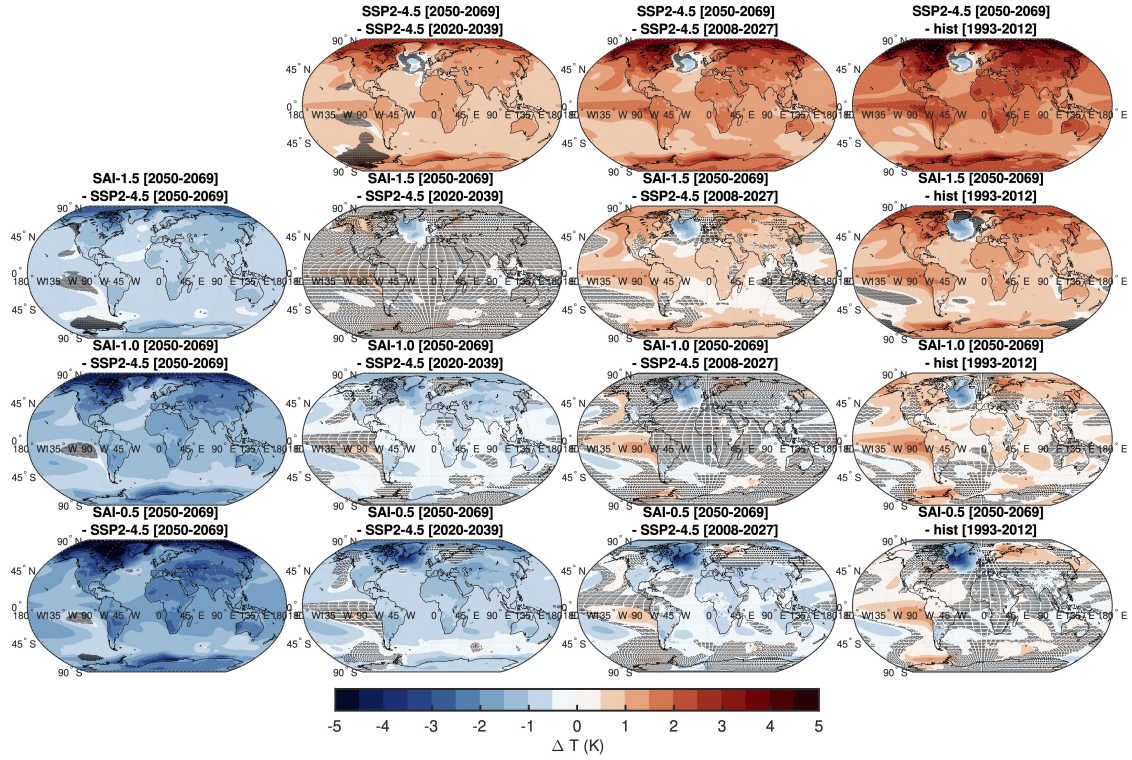


Figure 3. Comparison of surface temperatures changes averaged over 20 years periods and all ensemble members. The rows indicate the first term of the comparison, while the columns indicate the second. SSP2-4.5 [2050-2069] is both the first row and first column, indicating the reference future with an increase in CO₂ concentrations that is unabated by SAI. The other three rows show the three SAI simulations, from the one cooling the least (SAI-1.5) to the one cooling the most (SAI-0.5). The other three columns indicate the reference period selected, from the future to the historical period [1993-2012] (as simulated in CESM2-WACCM6).

348 lantic Meridional Overturning Circulation (AMOC). Both of these responses are ana-
 349 lyzed in more depth in Sections 3.2.1 and 3.3. Items of comparison outside of the diag-
 350 onal in Fig. 3 also offer valuable information. For instance, the comparison between SAI-
 351 1.5 and SSP2-4.5 (second row, third column) shows the results in which warming between
 352 SSP2-4.5 in 2050-2069 and BASE-1.0 (which equates to a 1.5°C temperature difference)
 353 is halved rather than considering it as an SAI case in which the whole warming from the
 354 period 2020-2039 is offset. In this case, one could argue that the cooling produced is mod-
 355 erate (P. Irvine et al., 2019; P. J. Irvine & Keith, 2020) (i.e. it doesn't offset the whole
 356 amount of warming) and thus would incur less SAI-induced changes (albeit most areas
 357 in such a strategy, by definition, would still be warmer than the period under compar-
 358 ison).

359 In general, we highlight that the particular choice of a baseline period can yield dif-
 360 ferent results, specifically in the perceptual sense of discussing if a particular feature looks
 361 “better” or “worse” under SAI, and while having a context in which to understand mech-
 362 anistic changes to climatic features is important (as we will discuss in the following sec-
 363 tions), it might always result in biased assessments of the role of SAI (Reynolds, 2022).
 364 It is crucial therefore to think of better ways to interpret changes due to SAI to make
 365 sure future assessments are more meaningful.

366 *3.2.1 Eastern tropical Pacific response*

367 El Niño/Southern Oscillation (ENSO) is one of the main climatic modes of vari-
 368 ability, the teleconnections of which have worldwide impacts (Timmermann et al., 2018).
 369 During El Niño periods an anomalous sea surface temperature (SST) warming pattern
 370 can be identified in the eastern/central Pacific, replaced by an anomalous SST cooling
 371 pattern during La Niña. These anomalies in the Pacific sea-surface temperatures are strongly
 372 coupled to changes in atmospheric convection and Walker Circulation, thereby affect-
 373 ing weather patterns on both sides of the Pacific Ocean. ENSO is a complex and highly
 374 variable phenomenon, and understanding its changes and impacts requires a detailed rep-
 375 resentation of a complex interplay of ocean and atmospheric processes.

376 Under GHG-induced warming, an increased equatorial Pacific warming and a weak-
 377 ening of the Walker circulation (Vecchi et al., 2006) are projected to lead to a stronger
 378 ENSO magnitude and frequency (Cai et al., 2015); this has been inferred through ENSO
 379 proxies (Grothe et al., 2020), reanalyses and multi-model projections (Cai et al., 2021).
 380 Given the need for long simulations in order to properly sample the underlying processes,
 381 provided the high variability and a comparatively long period of an average ENSO cy-
 382 cle, few results are available for SRM simulations. (Gabriel & Robock, 2015) examined
 383 a range of different GeoMIP G1-G4 experiments and found no statistically robust changes
 384 in ENSO characteristics under geoengineering compared to those driven by the GHGs
 385 alone. (Malik et al., 2020) used a 1000-year-long solar dimming simulation to assess changes
 386 in the mean state and extreme ENSO events, and found some significant changes com-
 387 pared to preindustrial. Such changes were, however, in large part driven by the tropi-
 388 cal overcooling typical of solar dimming simulations (Vioni, MacMartin, & Kravitz, 2021)
 389 and would thus not be representative of more complex SAI strategies maintaining mul-
 390 tiple surface temperature gradients such as those analyzed here.

391 In the absence of SAI, the simulated (20-year mean) SST pattern in the Pacific Ocean
 392 is similar to the positive phase of ENSO, (Fig. 3, first row), potentially due to similar
 393 mechanisms as the projected intensification of the El- Niño events under GHG-induced
 394 warming and the weakening of the Walker Circulation (see Section 3.4.1, Fig. 7) . De-
 395 spite the cancellation of the global mean surface temperature increase under SAI, when
 396 the different SAI scenarios are compared against each individual baseline period the sim-
 397 ulations still show increased SST in the eastern Pacific, suggestive also of a mean response
 398 with a pattern similar to the positive phase of ENSO that is not compensated by the SAI
 399 global cooling, statistically significant for SAI-1.0 and SAI-0.5 (diagonal maps in Fig. 3).

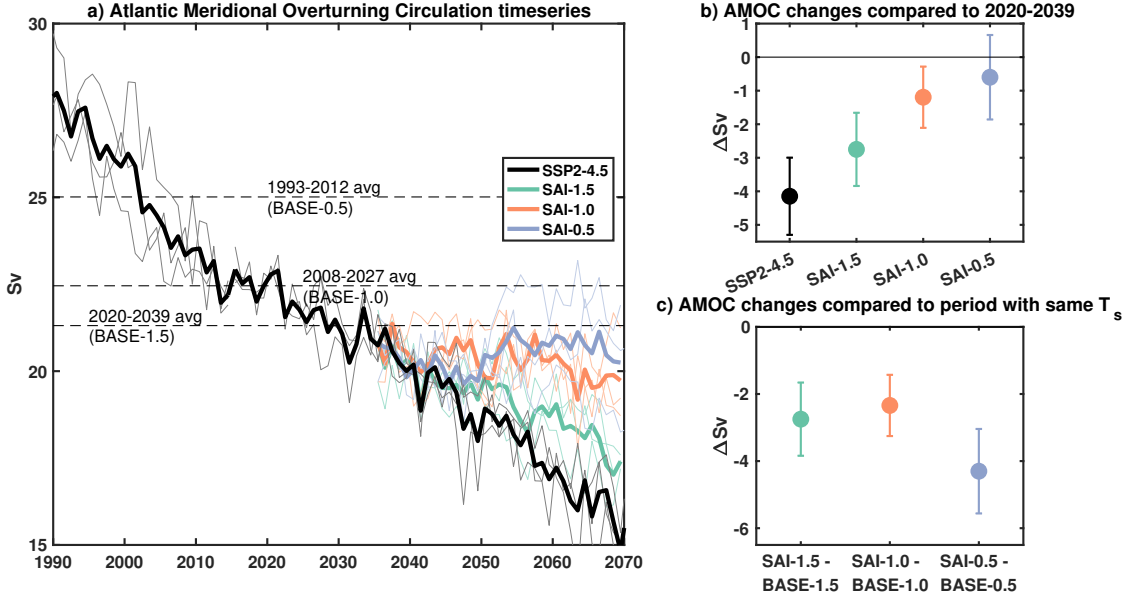


Figure 4. a) Yearly mean values of AMOC strength in all simulations, defined as the maximum value of the North Atlantic meridional overturning streamfunction. Lighter lines indicate single ensemble realizations, while thicker lines indicate the ensemble average. b) Changes in AMOC strength in 2050-2069 compared to the values in the period 2020-2039. The error bars indicate ± 1 standard error of the difference in means. c) Changes in AMOC strength in 2050-2069 for the three SAI simulations compared to their respective period with the same global mean surface temperature.

400

3.3 AMOC response

401

402

403

404

405

406

407

Fig. 4a shows a timeseries of the simulated AMOC strength, while Fig. 4b shows the associated twenty year average changes in 2050-2069 compared against the same quasi-present day BASE1.5 period and Fig. 4c shows the twenty year changes compared against each individual baseline period. In the absence of SAI, the strength of AMOC decreases under SSP2-4.5 because of the polar amplification and the resulting weakening of the temperature and salinity vertical gradients in the Northern Atlantic (Fasullo et al., 2018; Fasullo & Richter, 2023).

408

409

410

411

412

413

414

415

416

417

418

419

420

We find that all SAI scenarios slow AMOC weakening, with the effectiveness increasing marginally under increased magnitude of SAI. Importantly, the differences in the AMOC response among the three different SAI scenarios, when compared against the same BASE1.5 baseline period, are much smaller than the long-term GHG-induced AMOC trend under SSP2-4.5 alone when compared against the three different baseline periods. Thus, if one chooses to compare the SAI AMOC responses against their respective baseline periods the results show increased weakening under increased magnitude of SAI. In contrast, comparing the SAI AMOC responses against the same quasi-present day baseline period the results show reduced weakening under increased magnitude of SAI. This inconsistency is primarily driven by the differences in AMOC strength during the different reference periods, i.e. before SAI started. This analysis is another example presented here which highlights the importance of the chosen baseline period when evaluating the SAI responses under different magnitudes of global cooling.

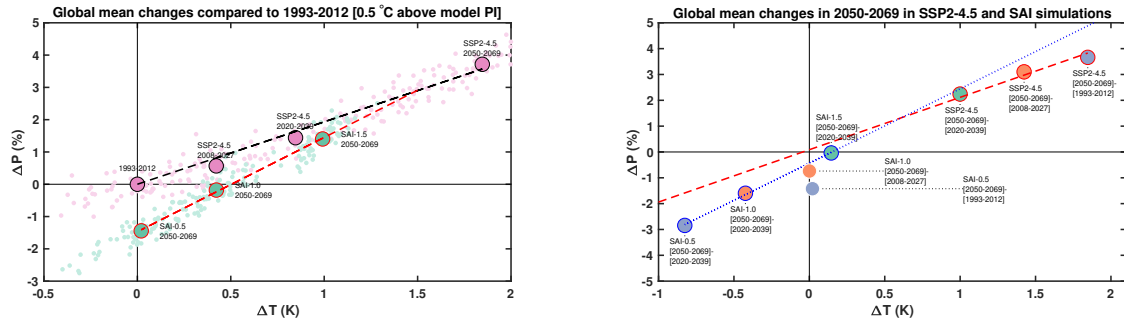


Figure 5. Changes in global mean temperature (K) compared to changes in precipitation (as a percent of the baseline precipitation, %), representing the Hydrological Sensitivity to both GHG-induced warming and SAI-induced cooling. In panel a), the values are represented against the coldest period analyzed in this work (1993-2012, 0.5°C above PI), for all three warmer periods due to GHG (2008-2027 for 1.0°C above PI; 2020-2039 for 1.5°C above PI; and 2050-2060 for 2.4°C above PI) and for the three SAI simulations in the period 2050-2069 with the three different levels of cooling. The single yearly values for each period and all ensemble members are also shown. In panel b), SAI values in 2050-2069 are compared against the 2020-2039 reference period, while the SSP2-4.5 values in 2050-2069 are compared against time periods which represent cooler temperatures in SSP2-4.5 in increments of 0.5°C.

421

3.4 Precipitation response

422

423

424

425

426

427

428

429

430

431

432

433

434

435

436

437

438

439

The precipitation response to changes in temperature has been previously investigated both for GHG-induced warming and for simulated SAI cooling. For abrupt 4xCO₂ experiments in the literature, this response can be typically divided into a fast (cloud, vegetation and radiative response to the perturbation) and a slow (usually identified with a temperature-driven response) contribution (Tilmes et al., 2013; Cao et al., 2015).

Under long-term changes in tropospheric temperatures, global mean precipitation tends to scale linearly with the surface temperatures. This relationship (called hydrological sensitivity, HS) can be explained in terms of changes to the energy balance of the atmosphere, and is a combination of the fast and slow response described above (Held & Soden, 2006; Pendergrass & Hartmann, 2014). The linearity of this response has been shown to hold in both modeling studies (Kvalevåg et al., 2013) and observational studies (DelSole et al., 2016), but with spread between individual models (Fläschner et al., 2016) and with considerable uncertainties over the available measurements (DelSole et al., 2016). In general, for the GHG-induced warming, the modeling consensus lies around 2-3% precipitation increase per 1 K of warming (Samset et al., 2018). For CESM, this is confirmed in Fig. 5 where we show a HS of 2.0% increase per K of warming in SSP2-4.5 as compared to the three reference periods with 1.5, 1.0 and 0.5 °C above the model PI.

440

441

442

443

444

445

446

447

448

For SRM, multiple modeling studies reported that for a certain amount of cooling, global precipitation would be reduced more compared to a GHG-induced increase (Niemeier et al., 2013; Tilmes et al., 2013), leading to what is usually termed as an “overcompensation of precipitation versus temperature”. Thermodynamical changes in the vertical temperature gradient is shown to be one of the reasons behind this, as the forcing from elevated CO₂ cannot be perfectly matched by a reduction in the incoming solar radiation, due to different mechanisms as the former warms from the bottom-up, and the latter cools from the top-down (Govindasamy et al., 2003; Ricke et al., 2023). Other reasons include the contribution of the aerosol-induced stratospheric heating under SAI (Simpson

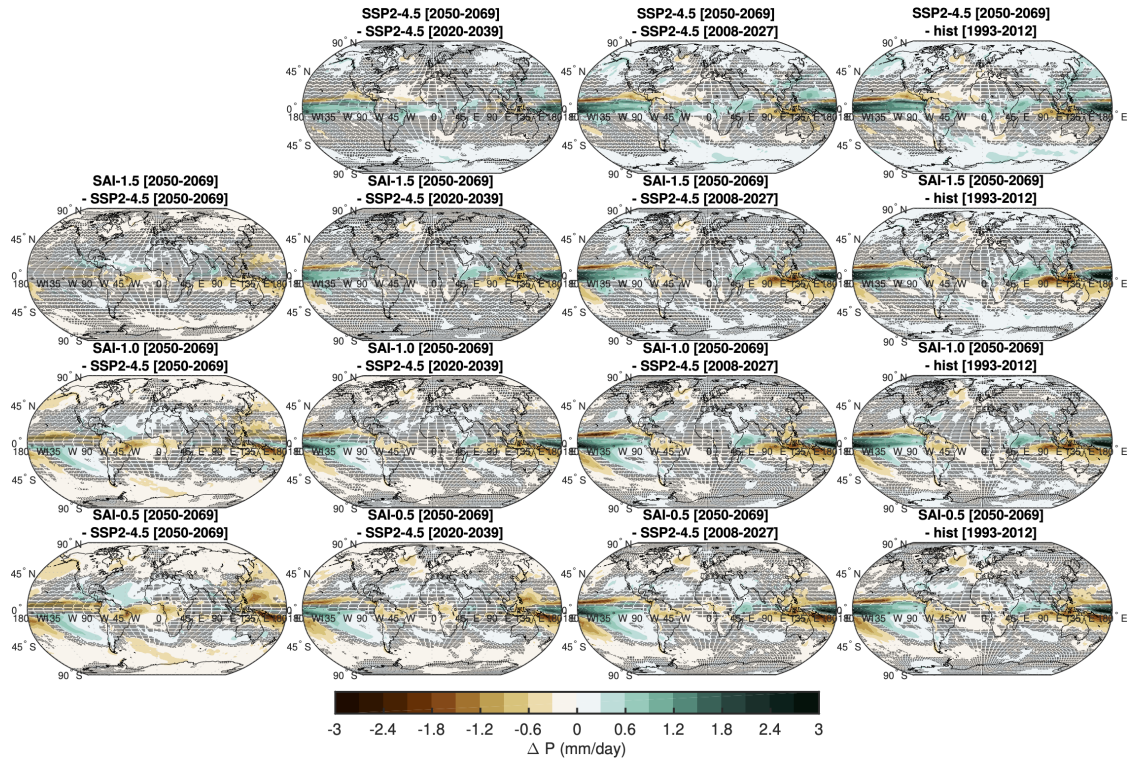


Figure 6. As in Fig. 3, but for the yearly mean precipitation response (mm/day).

449 et al., 2019; Visioni, MacMartin, & Kravitz, 2021) or differences between the land response to shortwave versus longwave forcing (Niemeier et al., 2013). As shown in Fig. 450 5, the SRM-specific changes are also confirmed in our simulations with different levels 451 of cooling as the slope of the linear fit for the SAI simulations when compared to the same 452 reference period (2020-2039) is steeper than the warming-derived one (2.9% decrease per 453 K of cooling). Similarly, when the SAI simulations are compared against their respective 454 baseline periods the difference between the two slopes is also evident. In these cases, 455 the data points for SAI-1.0 vs BASE-1.0 and SAI-0.5 vs BASE-0.5 indicate, by definition, 456 no changes in the global mean surface temperature; yet, the corresponding reduction 457 in the global mean precipitation grows larger with increasing levels of SAI. This change 458 in hydrological sensitivity induced by the compensation of GHG-warming with SAI can 459 be estimated to be equivalent to a 0.9% decrease per SAI-induced cooling. 460

461 3.4.1 Regional changes

462 Regionally, precipitation changes will reflect modulations of the large-scale tropo- 463 spheric circulation patterns. At this spatial scale, these changes are driven by the po- 464 sition and intensity of the Hadley (including the behavior of the Intertropical Conver- 465 gence Zone, ITCZ) and Walker Circulations as well as monsoonal circulation due to the 466 different temperature response between land (which warms or cools faster) and ocean.

467 The SSP2-4.5 precipitation response largely reflects the southward shift of the ITCZ 468 (Fig. S2) due to different rates of warming between the hemispheres, potentially also driven 469 by different tropospheric aerosol emissions (cite), alongside the overall increase in the 470 global mean precipitation caused by the increase in the global mean surface tempera- 471 tures. The combination of these two factors leads to an increase in yearly mean pre- 472 cipitation in equatorial Africa (Fig. 6). In the eastern Indian and western Pacific Ocean re- 473 gions, the weakening and eastward shift of the Walker Circulation in SSP2-4.5 (Fig. 7)

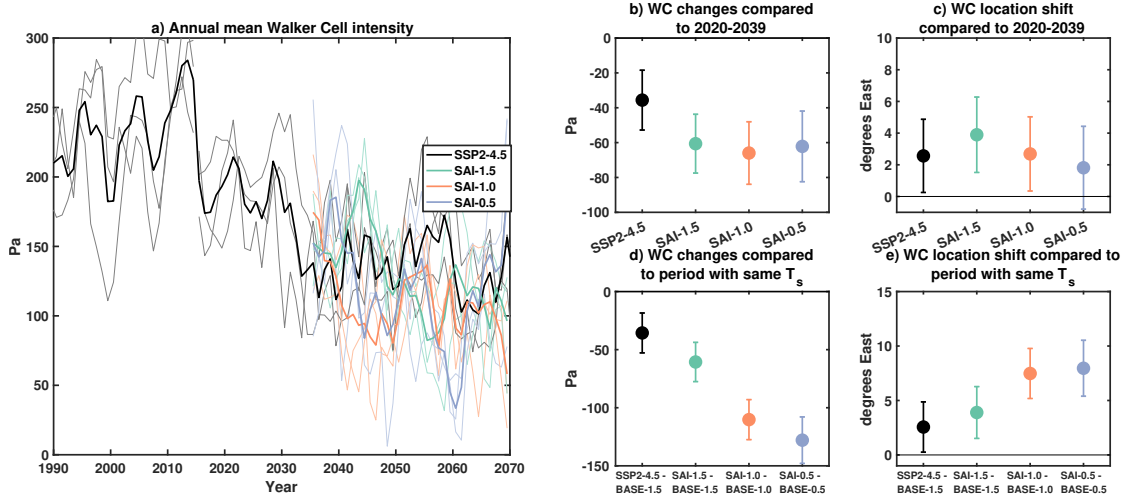


Figure 7. a) Annual mean Walker Circulation (WC) intensity for all experiments, with a 5-year moving average. b) Annual mean changes in the WC intensity from 2050-2069 compared to 2020-2039, and c) annual mean changes in the location of the transition between the anti-clockwise and the clockwise cells over the Indian Ocean and Western Pacific for the same time periods. d) Annual mean changes in the WC intensity for the three SAI simulations compared to each respective time period with the same global mean surface temperature, and e) annual mean changes in the location of the transition between the anticlockwise and the clockwise cells over the Indian Ocean and Western Pacific for the same time periods. The intensity of the Walker circulation is calculated using the SLP-base method (see text for details). The error bars indicate ± 1 standard error of the difference in means.

474 initiates a reduction in precipitation in the Indonesian region. We use two metrics of the
 475 Walker Circulation: i) a pressure based index of its intensity, defined as the difference
 476 in sea level pressure between east/central Pacific (160W-80W, 5S-5N) and western Pa-
 477 cific (80-160E, 5S-5N), as in Kang et al. (2020); and ii) the location of the individual cells
 478 of the Walker Circulation, estimated from the zonal mass streamfunction. The latter is
 479 calculated using the divergent component of zonal wind, averaged over 10S-10N, follow-
 480 ing the formula in (Guo et al., 2018). The longitudinal shift of the Walker Circulation
 481 is approximated by the shift of the zero line in the stream function at 400 hPa over the
 482 Indian Ocean and Western Pacific (80E-200E).

483 The weakening and eastward shift of Walker Circulation has been commonly simu-
 484 lated in climate models as a result of rising greenhouse gas levels and, thus, changes
 485 in static stability and lapse rate brought about by upper tropospheric temperature changes
 486 (e.g. Bayr et al. (2014); Nowack et al. (2015)). The weakening of the Walker Circula-
 487 tion under global warming is also consistent with the projected intensification of the El-
 488 Niño like events discussed in Section 3.2.1.

489 As discussed in Section 3.4, no significant change to global mean precipitation is
 490 simulated in SAI-1.5 (compared to 2020-2039), and the small decreases in SAI-1.0 and
 491 SAI-0.5 is due to the associated decreases in the global mean temperatures (Fig. 5). Re-
 492 garding the ITCZ position, the use of the feedback algorithm controlling the interhemi-
 493 spheric temperature gradient (T1) reduces the magnitude of the ITCZ shift in the SAI
 494 simulations compared to SSP2-4.5 (Fig. S2). Yet, a small ITCZ shift is nonetheless found
 495 in all SAI simulations illustrating that the feedback control over T1 is not a sufficient
 496 constraint. The magnitude of the ITCZ shift is however similar among the three SAI sce-
 497 narios.

498 Aside from the thermodynamically-driven changes in global mean precipitation and
499 those arising from shifts in the tropical zonal mean circulation and ITCZ, the SAI sim-
500 ulations also show relevant changes to the tropical Walker Circulation (Fig. 7). In par-
501 ticular, all three SAI simulations show a weakening and an eastward shift of the Walker
502 circulation, the magnitude of which increases with more cooling when the SAI simula-
503 tions are compared against their respective baseline period. In contrast, when compared
504 to the same quasi-present day baseline period, the SAI simulations show little change
505 to the strength or position of the Walker Circulation under increasing magnitude of SAI.
506 Notably, the sea-level pressure anomalies in the eastern Pacific strengthen under increas-
507 ing magnitude of SAI forcing but the anomalies in the western Pacific weaken (Fig. S4).
508 This result leads to similar changes of the Walker Circulation intensity across the three
509 SAI scenarios in Fig. 7 and suggests that factors other than global mean temperature
510 contribute to the Walker Circulation and precipitation response in the region under SAI.
511 The contrasting behavior which is dependent upon the baseline period likely reflects the
512 contribution of the GHG-induced changes in the Walker Circulation during the period
513 before SAI is started. These different baseline periods reflect different background (i.e.
514 non-SAI) forcings as shown by the large differences in the SSP2-4.5 responses as com-
515 pared to its temperature-dependent baseline periods (Fig. 7 and S3). This result high-
516 lights the importance of considering the baseline period when interpreting SAI impact
517 on Walker Circulation.

518 4 Conclusions

519 In this work, we presented results from multiple sets of Stratospheric Aerosol In-
520 jection (SAI) simulations in which SO_2 injections at four different latitudes are used to
521 maintain annual and global mean surface temperatures at 1.5, 1.0 and 0.5 °C above prein-
522 dustrial (PI) levels (SAI-1.5, SAI-1.0 and SAI-0.5 respectively) while greenhouse gas emis-
523 sions follow the CMIP6 SSP2-4.5 scenario.

524 The analyses serve to better understand the linearity of the climate response to the
525 different magnitudes of SAI. Furthermore, this work can help inform the design of an
526 emulator to be used to analyze comparatively large sets of SAI scenarios that would not
527 be computationally feasible using a fully-coupled Earth system model.

528 The three SAI scenarios all start SO_2 injections in 2035 and continue through 2069,
529 with analyses focusing on the last 20 years (2050-2069). For each of these SAI scenar-
530 ios, a corresponding 20-year-long baseline period is established from the SSP2-4.5 and/or
531 historical simulation (without SAI) that has the same global mean temperature: 2020-
532 2039 for SAI-1.5, 2008-2027 for SAI-1.0 and 1993-2012 for SAI-0.5. The choice of this
533 baseline period with the same global mean surface temperature permits an evaluation
534 of the diverse distribution of impacts arising from the imperfect compensation of the GHG-
535 induced warming with the cooling produced by the sulfate. Additionally, comparing the
536 SAI simulations against the same future period from the reference SSP2-4.5 scenario with-
537 out SAI facilitates an evaluation of the direct effectiveness of SAI compared to a future
538 climate modified by the GHG-induced warming. Finally, a comparison of the SAI sce-
539 narios and their impacts against the present day baseline period (here taken as 2020-2039)
540 provides valuable information for future SAI decision making processes. In addition to
541 stressing the importance of the choice of baseline period has for the context of the dis-
542 cussion, we also presented a couple of examples when the choice of baseline period can
543 spuriously affect the conclusions regarding the effectiveness and linearity of the SAI re-
544 sponses (e.g. on the strength of AMOC or Walker Circulation) under varying magnitudes
545 of the global mean surface cooling.

546 The main goal behind these simulations and of this work is to illustrate that an
547 evaluation of SAI impacts needs to take into account multiple dimensions in order to high-
548 light trade-offs and properly identify the space of possible SAI-driven impacts (MacMartin
549 et al., 2022). Here we have focused on the amount of cooling that SO_2 is chosen to pro-
550 duce, a method that is similar to the scenario exploration under different GHG concen-

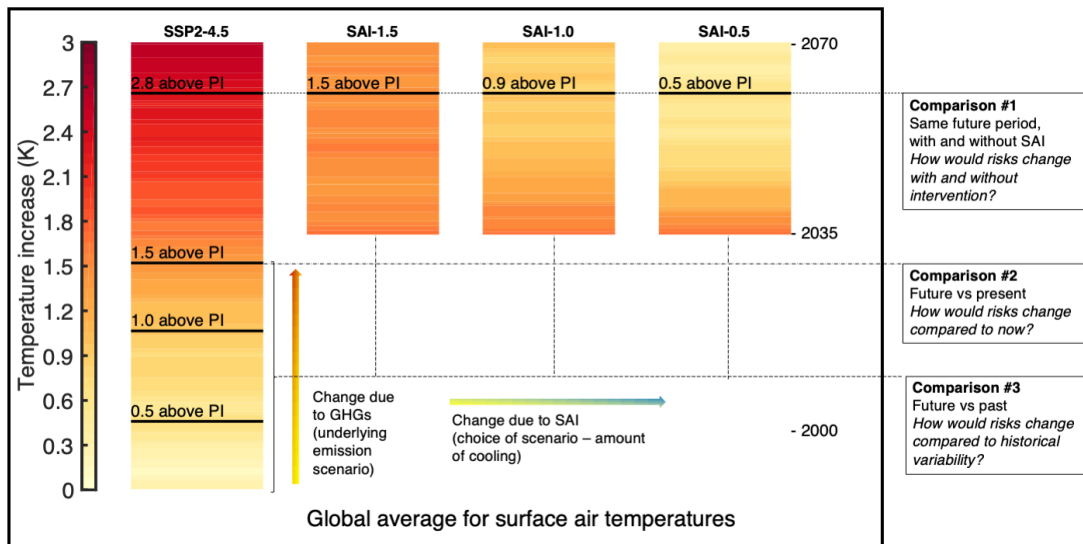


Figure 8. A schematic figure reflecting on the potential choices of comparison periods when discussing SAI impacts. Colorbar indicate global mean, ensemble mean average for surface temperature (K) as a deviation from the PI value.

551 trations in the IPCC scenarios (Meinshausen et al., 2020). In other works, the way in
 552 which some impacts are driven by different SO_2 injection locations (the injection strat-
 553 egy) has been explored (Kravitz et al., 2019; Vioni, MacMartin, Kravitz, Richter, et
 554 al., 2020; Bednarz et al., 2023; Zhang et al., 2023). Together these studies provide an
 555 overview of the possible design space of SAI that form a foundation for future SAI ex-
 556 plorations in a multi-model framework.

557 This work highlights that SAI studies, by adding a novel dimension to the ability
 558 to influence global warming impacts, need even more care when explaining how they are
 559 defining a certain simulated impact. Comparisons between different baseline periods can
 560 yield different insight onto what constitutes a direct SAI impacts, as opposed to what
 561 constitutes an imperfect compensation between GHG-induced warming and SAI: for in-
 562 stance, a change in tropospheric circulation due to stratospheric heating (Simpson et al.,
 563 2019; Bednarz et al., 2022) as opposed to the sea-land contrast not restored due to dif-
 564 ferent heat capacities resulting in monsoonal circulation changes (Vioni, MacMartin,
 565 Kravitz, Richter, et al., 2020). While such comparisons are fundamental for determin-
 566 ing some of the physical drivers (and thereby, might warrant SAI simulations with higher
 567 signal-to-noise ratio), it is hard to capture the nuance when discussing potential impacts
 568 and risks from a policy-relevant perspective. The choice of reference period is also rel-
 569 evant because people will interpret such comparison plots to infer influences on climate
 570 impacts, e.g., noting that some precipitation or temperature feature is over- or under-
 571 compensated relative to the compensation of global mean temperature; that SAI creates
 572 a “novel” climate state. In this sense, though, any choice of current or historical refer-
 573 ence period is potentially misleading: if some climate variable is restored to levels con-
 574 sistent with the past period when global mean temperature was 1.5°C above preindus-
 575 trial, and some other variable restored to levels consistent with an earlier historical pe-
 576 riod when global mean temperature was 1.0°C , it is entirely unobvious what the influ-
 577 ence of that novel climate state would have on human or ecosystem impacts, and the an-
 578 swer would depend on what changes have already been adapted to, for example. For this
 579 reason, it is important to stress that there is no single reference period relevant for in-

580 ferring ultimate impacts and indeed it may be more appropriate to compare to a range
581 of past conditions rather than to any single state (Figure 8).

582 5 Open Research

583 All model output analysed in this work is available at [https://doi.org/10.7298/xr82-](https://doi.org/10.7298/xr82-sv86)
584 [sv86](https://doi.org/10.7298/xr82-sv86) (Visioni, 2022).

585 Acknowledgments

586 We would like to acknowledge high-performance computing support from Cheyenne
587 (<https://doi.org/10.5065/D6RX99HX>) provided by NCAR's Computational and
588 Information Systems Laboratory, sponsored by the National Science Foundation. Sup-
589 port was provided by the NOAA cooperative agreement NA22OAR4320151, NOAA Earth's
590 Radiative Budget initiative, Cornell Atkinson Center for Sustainability, and by the Na-
591 tional Science Foundation through agreement CBET-2038246. Support for BK was pro-
592 vided in part by the National Science Foundation through agreement SES-1754740 and
593 the Indiana University Environmental Resilience Institute. The Pacific Northwest Na-
594 tional Laboratory is operated for the US Department of Energy by Battelle Memorial
595 Institute under contract DE-AC05-76RL01830.

596 References

- 597 Ban-Weiss, G. A., & Caldeira, K. (2010). Geoengineering as an optimization prob-
598 lem. *Environmental Research Letters*, *5*(3). doi: 10.1088/1748-9326/5/3/
599 034009
- 600 Bayr, T., Dommenges, D., Martin, T., & Power, S. B. (2014, November). The
601 eastward shift of the Walker Circulation in response to global warming and
602 its relationship to ENSO variability. *Climate Dynamics*, *43*(9), 2747–2763.
603 Retrieved from <https://doi.org/10.1007/s00382-014-2091-y> doi:
604 10.1007/s00382-014-2091-y
- 605 Bednarz, E. M., Butler, A. H., Visioni, D., Zhang, Y., Kravitz, B., & MacMartin,
606 D. G. (2023). Injection strategy – a driver of atmospheric circulation and
607 ozone response to stratospheric aerosol geoengineering. *EGUsphere*, *2023*,
608 1–32. Retrieved from [https://egusphere.copernicus.org/preprints/2023/](https://egusphere.copernicus.org/preprints/2023/egusphere-2023-495/)
609 egusphere-2023-495/ doi: 10.5194/egusphere-2023-495
- 610 Bednarz, E. M., Visioni, D., Richter, J. H., Butler, A. H., & MacMartin, D. G.
611 (2022). Impact of the latitude of stratospheric aerosol injection on the south-
612 ern annular mode. *Geophysical Research Letters*, *49*(19), e2022GL100353.
613 Retrieved from [https://agupubs.onlinelibrary.wiley.com/doi/abs/](https://agupubs.onlinelibrary.wiley.com/doi/abs/10.1029/2022GL100353)
614 [10.1029/2022GL100353](https://doi.org/10.1029/2022GL100353) (e2022GL100353 2022GL100353) doi: [https://](https://doi.org/10.1029/2022GL100353)
615 doi.org/10.1029/2022GL100353
- 616 Boettcher, M., Brent, K., Buck, H. J., Low, S., McLaren, D., & Mengis, N.
617 (2021). Navigating potential hype and opportunity in governing ma-
618 rine carbon removal. *Frontiers in Climate*, *3*. Retrieved from [https://](https://www.frontiersin.org/articles/10.3389/fclim.2021.664456)
619 www.frontiersin.org/articles/10.3389/fclim.2021.664456 doi:
620 10.3389/fclim.2021.664456
- 621 Brecha, R. J., Ganti, G., Lamboll, R. D., Nicholls, Z., Hare, B., Lewis, J., ... Gid-
622 den, M. J. (2022, August). Institutional decarbonization scenarios evaluated
623 against the Paris Agreement 1.5 °C goal. *Nature Communications*, *13*(1),
624 4304. Retrieved from <https://doi.org/10.1038/s41467-022-31734-1> doi:
625 10.1038/s41467-022-31734-1
- 626 Cai, W., Santoso, A., Collins, M., Dewitte, B., Karamperidou, C., Kug, J.-S., ...
627 Zhong, W. (2021, September). Changing El Niño–Southern Oscillation
628 in a warming climate. *Nature Reviews Earth & Environment*, *2*(9), 628–

- 629 644. Retrieved from <https://doi.org/10.1038/s43017-021-00199-z> doi:
630 10.1038/s43017-021-00199-z
- 631 Cai, W., Santoso, A., Wang, G., Yeh, S.-W., An, S.-I., Cobb, K. M., ... Wu, L.
632 (2015, September). ENSO and greenhouse warming. *Nature Climate Change*,
633 5(9), 849–859. Retrieved from <https://doi.org/10.1038/nclimate2743> doi:
634 10.1038/nclimate2743
- 635 Cao, L., Bala, G., Zheng, M., & Caldeira, K. (2015, December). Fast and slow
636 climate responses to CO₂ and solar forcing: A linear multivariate regression
637 model characterizing transient climate change. *Journal of Geophysical Re-*
638 *search: Atmospheres*, 120(23), 12,037–12,053. Retrieved 2023-05-24, from
639 <https://doi.org/10.1002/2015JD023901> (Publisher: John Wiley & Sons,
640 Ltd) doi: 10.1002/2015JD023901
- 641 Crutzen, P. J. (2006). Albedo enhancement by stratospheric sulfur injections:
642 A contribution to resolve a policy dilemma? *Climatic Change*, 77(3), 211–
643 220. Retrieved from <https://doi.org/10.1007/s10584-006-9101-y> doi:
644 10.1007/s10584-006-9101-y
- 645 Danabasoglu, G., Lamarque, J.-F., Bacmeister, J., Bailey, D. A., DuVivier, A. K.,
646 Edwards, J., ... Strand, W. G. (2020). The Community Earth System Model
647 Version 2 (CESM2). *Journal of Advances in Modeling Earth Systems*, 12(2),
648 e2019MS001916. doi: <https://doi.org/10.1029/2019MS001916>
- 649 Davis, N. A., Visioni, D., Garcia, R. R., Kinnison, D. E., Marsh, D. R., Mills, M. J.,
650 ... Vitt, F. (2022, dec). Climate, variability, and climate sensitivity of
651 “middle atmosphere” chemistry configurations of the community earth sys-
652 tem model version 2, whole atmosphere community climate model version 6
653 (CESM2(WACCM6)). Retrieved from [https://doi.org/10.22541/essoar](https://doi.org/10.22541/essoar.167117634.40175082/v1)
654 [.167117634.40175082/v1](https://doi.org/10.22541/essoar.167117634.40175082/v1) doi: 10.22541/essoar.167117634.40175082/v1
- 655 DelSole, T., Yan, X., & Tippet, M. K. (2016, September). Inferring Aerosol Cool-
656 ing from Hydrological Sensitivity. *Journal of Climate*, 29(17), 6167–6178.
657 Retrieved from [https://journals.ametsoc.org/view/journals/clim/29/
658 17/jcli-d-15-0364.1.xml](https://journals.ametsoc.org/view/journals/clim/29/17/jcli-d-15-0364.1.xml) (Place: Boston MA, USA Publisher: American
659 Meteorological Society) doi: 10.1175/JCLI-D-15-0364.1
- 660 Fasullo, J. T., & Richter, J. H. (2023). Dependence of strategic solar climate in-
661 tervention on background scenario and model physics. *Atmospheric Chemistry*
662 *and Physics*, 23(1), 163–182. Retrieved from [https://acp.copernicus.org/
663 articles/23/163/2023/](https://acp.copernicus.org/articles/23/163/2023/) doi: 10.5194/acp-23-163-2023
- 664 Fasullo, J. T., Simpson, I. R., Kravitz, B., Tilmes, S., Richter, J. H., MacMartin,
665 D. G., & Mills, M. J. (2018). Persistent polar ocean warming in a strate-
666 gically geoengineered climate. *Nature Geoscience*, 11(12), 910–914. Re-
667 trieved from <http://dx.doi.org/10.1038/s41561-018-0249-7> doi:
668 10.1038/s41561-018-0249-7
- 669 Fläschner, D., Mauritsen, T., & Stevens, B. (2016, January). Understanding the
670 Intermodel Spread in Global-Mean Hydrological Sensitivity. *Journal of Cli-*
671 *mate*, 29(2), 801–817. Retrieved from [https://journals.ametsoc.org/view/
672 journals/clim/29/2/jcli-d-15-0351.1.xml](https://journals.ametsoc.org/view/journals/clim/29/2/jcli-d-15-0351.1.xml) (Place: Boston MA, USA
673 Publisher: American Meteorological Society) doi: 10.1175/JCLI-D-15-0351.1
- 674 Gabriel, C. J., & Robock, A. (2015). Stratospheric geoengineering impacts on
675 El Niño/Southern Oscillation. *Atmospheric Chemistry and Physics*, 15(20),
676 11949–11966. Retrieved from [https://acp.copernicus.org/articles/15/
677 11949/2015/](https://acp.copernicus.org/articles/15/11949/2015/) doi: 10.5194/acp-15-11949-2015
- 678 Gao, Y., Gao, X., & Zhang, X. (2017). The 2 °c global temperature target
679 and the evolution of the long-term goal of addressing climate change—
680 from the united nations framework convention on climate change to the
681 paris agreement. *Engineering*, 3(2), 272-278. Retrieved from [https://
682 www.sciencedirect.com/science/article/pii/S2095809917303077](https://www.sciencedirect.com/science/article/pii/S2095809917303077) doi:
683 <https://doi.org/10.1016/J.ENG.2017.01.022>

- 684 Govindasamy, B., Caldeira, K., & Duffy, P. (2003). Geoengineering earth's ra-
 685 diation balance to mitigate climate change from a quadrupling of CO₂.
 686 *Global and Planetary Change*, 37(1), 157 - 168. Retrieved from [http://](http://www.sciencedirect.com/science/article/pii/S0921818102001959)
 687 www.sciencedirect.com/science/article/pii/S0921818102001959 (Eval-
 688 uation, Intercomparison and Application of Global Climate Models) doi:
 689 [https://doi.org/10.1016/S0921-8181\(02\)00195-9](https://doi.org/10.1016/S0921-8181(02)00195-9)
- 690 Grothe, P. R., Cobb, K. M., Liguori, G., Di Lorenzo, E., Capotondi, A., Lu, Y., ...
 691 Toth, L. T. (2020, April). Enhanced El Niño–Southern Oscillation Variabil-
 692 ity in Recent Decades. *Geophysical Research Letters*, 47(7), e2019GL083906.
 693 Retrieved 2023-05-24, from <https://doi.org/10.1029/2019GL083906> (Pub-
 694 lisher: John Wiley & Sons, Ltd) doi: 10.1029/2019GL083906
- 695 Guo, A., Moore, J. C., & Ji, D. (2018). Tropical atmospheric circulation re-
 696 sponse to the G1 sunshade geoengineering radiative forcing experiment.
 697 *Atmospheric Chemistry and Physics*, 18(12), 8689–8706. Retrieved
 698 from <https://acp.copernicus.org/articles/18/8689/2018/> doi:
 699 10.5194/acp-18-8689-2018
- 700 Haszeldine, R. S., Flude, S., Johnson, G., & Scott, V. (2018). Negative emissions
 701 technologies and carbon capture and storage to achieve the paris agreement
 702 commitments. *Philosophical Transactions of the Royal Society A: Mathemati-
 703 cal, Physical and Engineering Sciences*, 376(2119), 20160447. Retrieved from
 704 <https://royalsocietypublishing.org/doi/abs/10.1098/rsta.2016.0447>
 705 doi: 10.1098/rsta.2016.0447
- 706 Held, I. M., & Soden, B. J. (2006, November). Robust Responses of the Hydro-
 707 logical Cycle to Global Warming. *Journal of Climate*, 19(21), 5686–5699.
 708 Retrieved from [https://journals.ametsoc.org/view/journals/clim/19/](https://journals.ametsoc.org/view/journals/clim/19/21/jcli3990.1.xml)
 709 [21/jcli3990.1.xml](https://journals.ametsoc.org/view/journals/clim/19/21/jcli3990.1.xml) (Place: Boston MA, USA Publisher: American Meteorolo-
 710 gical Society) doi: 10.1175/JCLI3990.1
- 711 Holz, C., Siegel, L. S., Johnston, E., Jones, A. P., & Stermann, J. (2018, June).
 712 Ratcheting ambition to limit warming to 1.5 °C—trade-offs between emission re-
 713 ductions and carbon dioxide removal. *Environmental Research Letters*, 13(6),
 714 064028. Retrieved from <https://dx.doi.org/10.1088/1748-9326/aac0c1>
 715 (Publisher: IOP Publishing) doi: 10.1088/1748-9326/aac0c1
- 716 Irvine, P., Emanuel, K., He, J., Horowitz, L. W., Vecchi, G., & Keith, D. (2019).
 717 Halving warming with idealized solar geoengineering moderates key climate
 718 hazards. *Nature Climate Change*, 9(4), 295–299. Retrieved from [http://](http://dx.doi.org/10.1038/s41558-019-0398-8)
 719 dx.doi.org/10.1038/s41558-019-0398-8 doi: 10.1038/s41558-019-0398-8
- 720 Irvine, P. J., & Keith, D. W. (2020, mar). Halving warming with stratospheric
 721 aerosol geoengineering moderates policy-relevant climate hazards. *Environmen-
 722 tal Research Letters*, 15(4), 044011. Retrieved from [https://dx.doi.org/10](https://dx.doi.org/10.1088/1748-9326/ab76de)
 723 [.1088/1748-9326/ab76de](https://dx.doi.org/10.1088/1748-9326/ab76de) doi: 10.1088/1748-9326/ab76de
- 724 Irvine, P. J., Sriver, R. L., & Keller, K. (2012, February). Tension between reducing
 725 sea-level rise and global warming through solar-radiation management. *Nature
 726 Climate Change*, 2(2), 97–100. Retrieved from [https://doi.org/10.1038/](https://doi.org/10.1038/nclimate1351)
 727 [nclimate1351](https://doi.org/10.1038/nclimate1351) doi: 10.1038/nclimate1351
- 728 Kang, S. M., Xie, S.-P., Shin, Y., Kim, H., Hwang, Y.-T., Stuecker, M. F., ...
 729 Hawcroft, M. (2020). Walker circulation response to extratropical ra-
 730 diative forcing. *Science Advances*, 6(47), eabd3021. Retrieved from
 731 <https://www.science.org/doi/abs/10.1126/sciadv.abd3021> doi:
 732 10.1126/sciadv.abd3021
- 733 Kravitz, B., Lamarque, J.-F., Tribbia, J. J., Tilmes, S., Vitt, F., Richter, J. H., ...
 734 Mills, M. J. (2017). First Simulations of Designing Stratospheric Sulfate
 735 Aerosol Geoengineering to Meet Multiple Simultaneous Climate Objectives.
 736 *Journal of Geophysical Research: Atmospheres*, 122(23), 12,616–12,634. doi:
 737 10.1002/2017jd026874
- 738 Kravitz, B., MacMartin, D. G., Tilmes, S., Richter, J. H., Mills, M. J., Cheng, W.,

- 739 ... Vitt, F. (2019). Comparing surface and stratospheric impacts of geo-
 740 engineering with different SO₂ injection strategies. *Journal of Geophysi-
 741 cal Research: Atmospheres*, 124(14), 7900-7918. Retrieved from [https://
 742 agupubs.onlinelibrary.wiley.com/doi/abs/10.1029/2019JD030329](https://agupubs.onlinelibrary.wiley.com/doi/abs/10.1029/2019JD030329) doi:
 743 10.1029/2019JD030329
- 744 Kravitz, B., Robock, A., Tilmes, S., Boucher, O., English, J. M., Irvine, P. J.,
 745 ... Watanabe, S. (2015). The geoengineering model intercompari-
 746 son project phase 6 (GeoMIP6): simulation design and preliminary re-
 747 sults. *Geoscientific Model Development*, 8(10), 3379-3392. Retrieved
 748 from <https://gmd.copernicus.org/articles/8/3379/2015/> doi:
 749 10.5194/gmd-8-3379-2015
- 750 Krieglner, E., Luderer, G., Bauer, N., Baumstark, L., Fujimori, S., Popp, A., ... van
 751 Vuuren, D. P. (2018). Pathways limiting warming to 1.5°C: a tale of turn-
 752 ing around in no time? *Philosophical Transactions of the Royal Society A:
 753 Mathematical, Physical and Engineering Sciences*, 376(2119), 20160457. Re-
 754 trieved from [https://royalsocietypublishing.org/doi/abs/10.1098/
 755 rsta.2016.0457](https://royalsocietypublishing.org/doi/abs/10.1098/rsta.2016.0457) doi: 10.1098/rsta.2016.0457
- 756 Kvalevåg, M. M., Samset, B. H., & Myhre, G. (2013, April). Hydrological sensi-
 757 tivity to greenhouse gases and aerosols in a global climate model. *Geophysical
 758 Research Letters*, 40(7), 1432-1438. Retrieved 2023-05-24, from [https://doi
 759 .org/10.1002/grl.50318](https://doi.org/10.1002/grl.50318) (Publisher: John Wiley & Sons, Ltd) doi: 10.1002/
 760 grl.50318
- 761 Laakso, A., Niemeier, U., Visoni, D., Tilmes, S., & Kokkola, H. (2022). Dependency
 762 of the impacts of geoengineering on the stratospheric sulfur injection strategy –
 763 part 1: Intercomparison of modal and sectional aerosol modules. *Atmospheric
 764 Chemistry and Physics*, 22(1), 93-118.
- 765 Lenton, T. M., Held, H., Krieglner, E., Hall, J. W., Lucht, W., Rahmstorf, S., &
 766 Schellnhuber, H. J. (2008). Tipping elements in the earth's climate system.
 767 *Proceedings of the National Academy of Sciences*, 105(6), 1786-1793. Retrieved
 768 from <https://www.pnas.org/doi/abs/10.1073/pnas.0705414105> doi:
 769 10.1073/pnas.0705414105
- 770 Liu, X., Ma, P.-L., Wang, H., Tilmes, S., Singh, B., Easter, R. C., ... Rasch,
 771 P. J. (2016). Description and evaluation of a new four-mode version of the
 772 Modal Aerosol Module (MAM4) within version 5.3 of the Community At-
 773 mosphere Model. *Geoscientific Model Development*, 9(2), 505-522. doi:
 774 10.5194/gmd-9-505-2016
- 775 MacMartin, D. G., Kravitz, B., Mills, M. J., Tribbia, J. J., Tilmes, S., Richter,
 776 J. H., ... Lamarque, J.-F. (2017). The Climate Response to Stratospheric
 777 Aerosol Geoengineering Can Be Tailored Using Multiple Injection Locations.
 778 *Journal of Geophysical Research: Atmospheres*, 122(23), 12,574-12,590. doi:
 779 10.1002/2017jd026868
- 780 MacMartin, D. G., Ricke, K. L., & Keith, D. W. (2018). Solar geoengineer-
 781 ing as part of an overall strategy for meeting the 1.5°C paris tar-
 782 get. *Philosophical Transactions of the Royal Society A: Mathematical,
 783 Physical and Engineering Sciences*, 376(2119), 20160454. Retrieved from
 784 <https://royalsocietypublishing.org/doi/abs/10.1098/rsta.2016.0454>
 785 doi: 10.1098/rsta.2016.0454
- 786 MacMartin, D. G., Visoni, D., Kravitz, B., Richter, J., Felgenhauer, T., Lee, W. R.,
 787 ... Sugiyama, M. (2022). Scenarios for modeling solar radiation modification.
 788 *Proceedings of the National Academy of Sciences*, 119(33), e2202230119. Re-
 789 trieved from <https://www.pnas.org/doi/abs/10.1073/pnas.2202230119>
 790 doi: 10.1073/pnas.2202230119
- 791 Malik, A., Nowack, P. J., Haigh, J. D., Cao, L., Atique, L., & Plancherel, Y. (2020).
 792 Tropical Pacific climate variability under solar geoengineering: impacts on
 793 ENSO extremes. *Atmospheric Chemistry and Physics*, 20(23), 15461-15485.

- 794 Retrieved from <https://acp.copernicus.org/articles/20/15461/2020/>
795 doi: 10.5194/acp-20-15461-2020
- 796 Masson-Delmotte, V., et al. (Eds.). (2018). *Global Warming of 1.5°C: An IPCC*
797 *Special Report on the impacts of global warming of 1.5°C above pre-industrial*
798 *levels and related global greenhouse gas emission pathways, in the context of*
799 *strengthening the global response to the threat of climate change, sustainable*
800 *development, and efforts to eradicate poverty.* Geneva, Switzerland: World
801 Meteorological Organization. Retrieved from <https://www.ipcc.ch/sr15/>
- 802 Meinshausen, M., Nicholls, Z. R. J., Lewis, J., Gidden, M. J., Vogel, E., Freund, M.,
803 ... Wang, R. H. J. (2020). The shared socio-economic pathway (ssp) green-
804 house gas concentrations and their extensions to 2500. *Geoscientific Model De-*
805 *velopment*, 13(8), 3571–3605. Retrieved from [https://gmd.copernicus.org/](https://gmd.copernicus.org/articles/13/3571/2020/)
806 [articles/13/3571/2020/](https://gmd.copernicus.org/articles/13/3571/2020/) doi: 10.5194/gmd-13-3571-2020
- 807 Niemeier, U., Schmidt, H., Alterskjær, K., & Kristjánsson, J. E. (2013). Solar
808 irradiance reduction via climate engineering: Impact of different techniques
809 on the energy balance and the hydrological cycle. *Journal of Geophysical*
810 *Research: Atmospheres*, 118(21), 11,905–11,917. Retrieved from [https://](https://agupubs.onlinelibrary.wiley.com/doi/abs/10.1002/2013JD020445)
811 agupubs.onlinelibrary.wiley.com/doi/abs/10.1002/2013JD020445 doi:
812 10.1002/2013JD020445
- 813 Niemeier, U., & Timmreck, C. (2015). What is the limit of climate engineering by
814 stratospheric injection of SO₂? *Atmospheric Chemistry and Physics*, 15(16),
815 9129–9141. Retrieved from [https://www.atmos-chem-phys.net/15/9129/](https://www.atmos-chem-phys.net/15/9129/2015/)
816 [2015/](https://www.atmos-chem-phys.net/15/9129/2015/) doi: 10.5194/acp-15-9129-2015
- 817 Nowack, P. J., Luke Abraham, N., Maycock, A. C., Braesicke, P., Gregory, J. M.,
818 Joshi, M. M., ... Pyle, J. A. (2015, January). A large ozone-circulation
819 feedback and its implications for global warming assessments. *Nature Cli-*
820 *mate Change*, 5(1), 41–45. Retrieved from [https://doi.org/10.1038/](https://doi.org/10.1038/nclimate2451)
821 [nclimate2451](https://doi.org/10.1038/nclimate2451) doi: 10.1038/nclimate2451
- 822 Pendergrass, A. G., & Hartmann, D. L. (2014, January). The Atmospheric Energy
823 Constraint on Global-Mean Precipitation Change. *Journal of Climate*, 27(2),
824 757–768. Retrieved from [https://journals.ametsoc.org/view/journals/](https://journals.ametsoc.org/view/journals/clim/27/2/jcli-d-13-00163.1.xml)
825 [clim/27/2/jcli-d-13-00163.1.xml](https://journals.ametsoc.org/view/journals/clim/27/2/jcli-d-13-00163.1.xml) (Place: Boston MA, USA Publisher:
826 American Meteorological Society) doi: 10.1175/JCLI-D-13-00163.1
- 827 Rajamani, L., & Werksman, J. (2018). The legal character and operational relevance
828 of the paris agreement's temperature goal. *Philosophical Transactions of the*
829 *Royal Society A: Mathematical, Physical and Engineering Sciences*, 376(2119),
830 20160458. Retrieved from [https://royalsocietypublishing.org/doi/abs/](https://royalsocietypublishing.org/doi/abs/10.1098/rsta.2016.0458)
831 [10.1098/rsta.2016.0458](https://royalsocietypublishing.org/doi/abs/10.1098/rsta.2016.0458) doi: 10.1098/rsta.2016.0458
- 832 Reynolds, J. L. (2022). Communication of solar geoengineering science:
833 Forms, examples, and explanation of skewing. *The Anthropocene Review*,
834 0(0), 20530196221095569. Retrieved from [https://doi.org/10.1177/](https://doi.org/10.1177/20530196221095569)
835 [20530196221095569](https://doi.org/10.1177/20530196221095569) doi: 10.1177/20530196221095569
- 836 Ricke, K., Wan, J. S., Saenger, M., & Lutsko, N. J. (2023). Hydrological conse-
837 quences of solar geoengineering. *Annual Review of Earth and Planetary Sci-*
838 *ences*, 51(1), null. Retrieved from [https://doi.org/10.1146/annurev-earth](https://doi.org/10.1146/annurev-earth-031920-083456)
839 [-031920-083456](https://doi.org/10.1146/annurev-earth-031920-083456) doi: 10.1146/annurev-earth-031920-083456
- 840 Robock, A., Oman, L., & Stenchikov, G. L. (2008). Regional climate responses
841 to geoengineering with tropical and arctic so₂ injections. *Journal of Geo-*
842 *physical Research: Atmospheres*, 113(D16). Retrieved from [https://](https://agupubs.onlinelibrary.wiley.com/doi/abs/10.1029/2008JD010050)
843 agupubs.onlinelibrary.wiley.com/doi/abs/10.1029/2008JD010050 doi:
844 <https://doi.org/10.1029/2008JD010050>
- 845 Samset, B. H., Myhre, G., Forster, P. M., Hodnebrog, Ø., Andrews, T., Boucher,
846 O., ... Voulgarakis, A. (2018, January). Weak hydrological sensitivity to
847 temperature change over land, independent of climate forcing. *npj Climate*
848 *and Atmospheric Science*, 1(1), 20173. Retrieved from <https://doi.org/>

- 10.1038/s41612-017-0005-5 doi: 10.1038/s41612-017-0005-5
- 849 Simpson, I., Tilmes, S., Richter, J., Kravitz, B., MacMartin, D., Mills, M., ...
850 Pendergrass, A. (2019). The regional hydroclimate response to strato-
851 spheric sulfate geoengineering and the role of stratospheric heating. *Jour-
852 nal of Geophysical Research: Atmospheres*, 2019JD031093. Retrieved from
853 <https://onlinelibrary.wiley.com/doi/abs/10.1029/2019JD031093> doi:
854 10.1029/2019JD031093
855
- 856 Tilmes, S., Fasullo, J., Lamarque, J.-F., Marsh, D. R., Mills, M., Alterskjær, K.,
857 ... Watanabe, S. (2013). The hydrological impact of geoengineering in the
858 geoengineering model intercomparison project (GeoMIP). *Journal of Geo-
859 physical Research: Atmospheres*, 118(19), 11,036-11,058. Retrieved from
860 <https://agupubs.onlinelibrary.wiley.com/doi/abs/10.1002/jgrd.50868>
861 doi: 10.1002/jgrd.50868
- 862 Timmermann, A., An, S.-I., Kug, J.-S., Jin, F.-F., Cai, W., Capotondi, A., ...
863 Zhang, X. (2018, July). El Niño–Southern Oscillation complexity. *Na-
864 ture*, 559(7715), 535–545. Retrieved from [https://doi.org/10.1038/
865 s41586-018-0252-6](https://doi.org/10.1038/s41586-018-0252-6) doi: 10.1038/s41586-018-0252-6
- 866 Vecchi, G. A., Soden, B. J., Wittenberg, A. T., Held, I. M., Leetmaa, A., & Harri-
867 son, M. J. (2006, May). Weakening of tropical Pacific atmospheric circulation
868 due to anthropogenic forcing. *Nature*, 441(7089), 73–76. Retrieved from
869 <https://doi.org/10.1038/nature04744> doi: 10.1038/nature04744
- 870 Visioni, D. (2022). *Data from: Scenarios for modeling solar radiation modification*.
871 doi: <https://doi.org/10.7298/xr82-sv86>
- 872 Visioni, D., Bednarz, E. M., Lee, W. R., Kravitz, B., Jones, A., Haywood, J. M., &
873 MacMartin, D. G. (2023). Climate response to off-equatorial stratospheric
874 sulfur injections in three earth system models – part 1: Experimental protocols
875 and surface changes. *Atmospheric Chemistry and Physics*, 23(1), 663–685.
876 Retrieved from <https://acp.copernicus.org/articles/23/663/2023/> doi:
877 10.5194/acp-23-663-2023
- 878 Visioni, D., MacMartin, D. G., & Kravitz, B. (2021). Is turning down the sun a
879 good proxy for stratospheric sulfate geoengineering? *Journal of Geophysical
880 Research: Atmospheres*, 126(5), e2020JD033952. Retrieved from [https://
881 agupubs.onlinelibrary.wiley.com/doi/abs/10.1029/2020JD033952](https://agupubs.onlinelibrary.wiley.com/doi/abs/10.1029/2020JD033952)
882 (e2020JD033952 2020JD033952) doi: <https://doi.org/10.1029/2020JD033952>
- 883 Visioni, D., MacMartin, D. G., Kravitz, B., Boucher, O., Jones, A., Lurton, T.,
884 ... Tilmes, S. (2021). Identifying the sources of uncertainty in climate
885 model simulations of solar radiation modification with the g6sulfur and
886 g6solar geoengineering model intercomparison project (geomip) simula-
887 tions. *Atmospheric Chemistry and Physics*, 21(13), 10039–10063. Re-
888 trieved from <https://acp.copernicus.org/articles/21/10039/2021/>
889 doi: 10.5194/acp-21-10039-2021
- 890 Visioni, D., MacMartin, D. G., Kravitz, B., Lee, W., Simpson, I. R., & Richter,
891 J. H. (2020). Reduced poleward transport due to stratospheric heating under
892 stratospheric aerosols geoengineering. *Geophysical Research Letters*, n/a(n/a),
893 e2020GL089470. Retrieved from [https://agupubs.onlinelibrary.wiley
894 .com/doi/abs/10.1029/2020GL089470](https://agupubs.onlinelibrary.wiley.com/doi/abs/10.1029/2020GL089470) (e2020GL089470 2020GL089470) doi:
895 10.1029/2020GL089470
- 896 Visioni, D., MacMartin, D. G., Kravitz, B., Richter, J. H., Tilmes, S., & Mills, M. J.
897 (2020). Seasonally modulated stratospheric aerosol geoengineering alters the
898 climate outcomes. *Geophysical Research Letters*, n/a(n/a), e2020GL088337.
899 Retrieved from [https://agupubs.onlinelibrary.wiley.com/doi/abs/
900 10.1029/2020GL088337](https://agupubs.onlinelibrary.wiley.com/doi/abs/10.1029/2020GL088337) (e2020GL088337 2020GL088337) doi: 10.1029/
901 2020GL088337
- 902 Warszawski, L., Kriegler, E., Lenton, T. M., Gaffney, O., Jacob, D., Klingen-
903 feld, D., ... Rockström, J. (2021, May). All options, not silver bullets,

904 needed to limit global warming to 1.5 °C: a scenario appraisal. *Envi-*
905 *ronmental Research Letters*, 16(6), 064037. Retrieved from [https://](https://dx.doi.org/10.1088/1748-9326/abfeec)
906 dx.doi.org/10.1088/1748-9326/abfeec (Publisher: IOP Publishing) doi:
907 10.1088/1748-9326/abfeec
908 Zhang, Y., MacMartin, D. G., Vioni, D., Bednarz, E., & Kravitz, B. (2023).
909 Introducing a Comprehensive Set of Stratospheric Aerosol Injection Strate-
910 gies. *EGUsphere*, 2023, 1–32. Retrieved from [https://egusphere](https://egusphere.copernicus.org/preprints/2023/egusphere-2023-117/)
911 [.copernicus.org/preprints/2023/egusphere-2023-117/](https://egusphere.copernicus.org/preprints/2023/egusphere-2023-117/) doi: 10.5194/
912 egusphere-2023-117